PAPER

Active Contour Using Local Regional Information on Extendable Search Lines (LRES) for Image Segmentation

Sopon PHUMEECHANYA[†a)], ***Student Member***, **Charnchai PLUEMPITIWIRIYAWEJ**[†*b)], ***and*** **Saowapak THONGVIGITMANEE**[††c)], ***Nonmembers***

SUMMARY In this paper, we propose a novel active contour method for image segmentation using a local regional information on extendable search line. We call it the **LRES** active contour. Our active contour uses the intensity values along a set of search lines that are perpendicular to the contour front. These search lines are used to inform the contour front toward which direction to move in order to find the object's boundary. Unlike other methods, none of these search lines have a predetermined length. Instead, their length increases gradually until a boundary of the object is found. We compare the performance of our LRES active contour to other existing active contours, both edge-based and region-based. The results show that our method provides more desirable segmentation outcomes, particularly on some images where other methods may fail. Not only is our method robust to noise and able to reach into a deep concave shape, it also has a large capture range and performs well in segmenting heterogeneous textured objects.

key words: *active contours, image segmentation, level set, search line, snakes*

1. Introduction

Active contours or snakes [1] have been used broadly in image segmentation. The contours move and deform within the image domain under a combined influence of internal and external forces. The internal force refers to the self-generated force that controls the smoothness of the contour during the deformation. The external force is usually derived from the image and acts as a gravitational field to pull the contour toward the boundary of the desired object within the image. The external force may be categorized into the edge-based [1]–[7] and the region-based [8]–[16] approaches. The edge-based force employs local edge information, e.g. the image gradient, as a clue to find the object boundary. The region-based force generally uses the difference between regional statistics of the image, a more global type of information than edges, to guide the motion of the active contour toward the object of interest.

The traditional active contour model (TAC) or snake, introduced by Kass et al. [1], utilizes the gradient vector of the image's edge map. It is known to be quite sensitive to noise, unable to reach any deep concavity, and has poor capture range [2]. Therefore, the contour must be initially placed not too far from the actual boundary of the object for the TAC to work properly. Many methods have been proposed to improve the snake's performance. Distance vector flow (DVF) by Cohen and Cohen [2] uses the gradient vectors of the Euclidean distance between each image pixel and the nearest pixel of candidate edges. As a result, it has a longer capture range to object's boundary. However, it still cannot trace shapes with deep concave parts. Xu and Prince [3] proposed the gradient vector flow (GVF) method that spatially diffuses the gradient of the image's edge map so that each vector in the force field is extended gradually. As a result, it solves the problems of limited capture range and poor reachability into concave parts. However, the GVF method suffers from high computational requirement. Li and Acton [4] introduced an edge-based force called the vector field convolution (VFC) that convolves the edge map generated from the image with a vector field kernel. Similar to the GVF, the VFC provides large capture range and the ability to navigate into the concave part of the object boundary. Yet, it is less computationally expensive and more robust to noise than the GVF [3]. Wang and Zhang [5] proposed the Coulomb active contour model (CAC). Their edge-based force is based on the Coulomb's law in static electric theory. The Coulomb force at any position on the image is the vector sum of the Coulomb forces affected by all the candidate edge pixels. The CAC method provides a larger capture range with low computational complexity but it sometimes, as we shall see in experiment section, cannot extract concaved objects correctly.

Furthermore, all of these edge-based active contour methods often inevitably suffer from the saddle point and stationary point problems [6]. For example, Fig. 1 (a) shows a U shape image with a small opening at the concave part and its VFC vector field is shown in Fig. 1 (b). We can clearly see in Fig. 1 (c) that there is a saddle point at the "bottleneck" region, as shown within the rectangle. The vectors within this region form a "wall" that obstructs the active contour to pass inside. In addition, there is a stationary point at the "bay" region, as shown within the circle in Fig. 1 (c). All of the vectors within the "bay" region are pointing outwards in all directions to the nearest edge points. As a result, these two points are crucial obstacles for the active contour to move pass the stationary point and go toward the innermost part of the U shape as shown in column (b) of Fig. 4

Manuscript received September 12, 2009.
Manuscript revised January 26, 2010.

[†]The authors are with the Department of Electrical Engineering, Chulalongkorn University, Bangkok, Thailand.
[††]The author is with National Electronics and Computer Technology Center, Pathumthani, Thailand.
[*]Corresponding Author
a) E-mail: sopon.p@student.chula.ac.th
b) E-mail: charnchai.p@chula.ac.th
c) E-mail: saowapak.thongvigitmanee@nectec.or.th

DOI: 10.1587/transinf.E93.D.1625

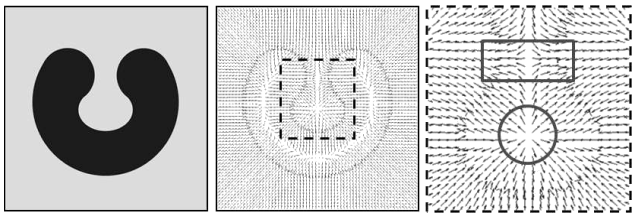

(a) (b) (c)

Fig. 1 (a) a U shape image (b) the VFC vector filed of the image (c) saddle point (in rectangle) and stationary point (in circle).

(a) (b) (c)

Fig. 2 (a) an example of the heterogeneous textured object (b) the segmentation result of the image using global region-based active contour (the ACWE [8]) and (c) the two-shade version of the result.

in the experiment section. Our newly proposed method (the LRES active contour), however, is designed to solve these problems, while keeping the advantages of existing methods.

Besides the edge-based forces, region-based forces are often used in active contour schemes for image segmentation. In region-based force models, the entire image information is statistically calculated. The active contours then use this information to segment the image into the object and the background regions. These regional statistic models are more global than the edge-based models where only few pixels in the gradient image are considered as the boundary candidates. As a result, it is less sensitive to noise and more robust to initialization than the edge-based counterpart. Moreover, they perform well even in the images with low signal-to-noise ratio. There are many active contour methods that take into account the region-based force. For instance, Chan and Vese [8] introduced a powerful "Active Contour Without Edge" (ACWE). They integrated the level set method [17] and the Mumford-Shah model [18] to obtain an energy function that is based on the average intensities of the pixels within the object and the background areas. Their energy is optimized when the average pixel intensities of the interior and the exterior of the contour are well separated. Yezzi et al. [9] proposed a similar scheme but they use the regional variances instead. The optimum point of their energy function is accomplished when the variances inside and outside the contour are most different. Recently, Michailovich et al. [10] introduced an energy function that compares the histograms of the foreground and the background based on the Bhattacharyya distance [19]. This energy is minimized when the Bhattacharyya distance between the probability density functions inside and outside the evolving contour is the smallest.

In the case where the object or the background are of heterogeneous textures, however, the region-based methods with such global constrain may not perform effectively. As shown in Fig. 2 (a), for example, the object has non-uniform texture. When we apply such global region-based active contour as the ACWE [8], it results in a delusive segmentation as shown in Fig. 2 (b). The contour attempts to separate the image into the light region and the dark region as shown in the two-shade version in Fig. 2 (c), which is not quite of our desire, which is the triangular-like shape object in the center of the image. An ability to segment heterogeneous textured objects is very important because heterogeneous textured objects exist in many medical images and natural scenes.

To overcome the limitation of the global region-based method in segmenting an image where the object or the background or both are of heterogeneous textures, several methods have utilized some local regional information as a constrain to the active contour. For instance, Mille and Cohen [14] proposed the local normal-based region term (LNBR) for active contours. This method does not use the entire regional information on the image, but rather it uses the intensity of only the pixels inside and on the closed proximity outside the contour, i.e., "the outer band". This method is designed to segment only the case of a homogeneous textured object lying within a heterogeneous textured background. Ronfard [15] introduced a local region-based active contour model that employs regions only around the neighborhoods band, both inside and outside, of the contour. Although this method can segment a heterogeneous textured object, the initial contour must be placed not far from the boundary of the object than predetermined within of the neighborhood band. Recently, Lankton and Tannenbaum [16] proposed the localizing region-based active contours called LRAC. This method uses the local regional information that is within the circles that are around the contour. The centers of these circles are the pixels on the contour. The radii of all circles are set priori by a user. Setting the radius parameter depends on the distance between the positions of the initial contour and the object within the image. If the initial contour is placed too far from the boundary of the object and the radius of the circle is too small, the contour still cannot move toward the object's boundary. In other words, the method may not have enough capture range if the radius parameter is too small. On the other hand, if the radius parameter is set too large, the method may act like a global active contour and it may not be able to segment a heterogeneous textured object correctly. In practice, it is difficult to set a suitable radius parameter for an object, especially when it has several concave parts.

In this paper, we propose a new active contour method to overcome the limitations of the previous edge-based and region-based active contours. Rather than using the edge map, our method uses intensity profile of the pixels along the search line that is perpendicular to the contour front. Then, a force similar to the region-based force, but more

local, is determined in each search line, thus preserving the advantages of the region-based methods. Moreover, to increase the capture range, each search line is not of fixed length. Its length increases according to the obtained local information. The local region-based force with extendable search line provides us with many advantages as follows: 1) a large capture range, 2) an ability to handle concave shapes, 3) non-existence of the saddle and stationary point problems, 4) robustness to noise, and 5) an ability to segment heterogeneous textured object.

The remainder of this paper is organized as follows. Section 2 provides a brief review of the fixed-length search line method [7] and the global region-based active contour [8]. The proposed method is then described in Sect.,3. Experimental results and comparison appear in Sect. 4. Finally, conclusion is drawn in Sect. 5.

2. Background

2.1 Fixed-Length Search Line Method

Our extendable search line method (described in Sect.3.1) is motivated by the work of Cootes et al. [7]. Their active contour uses search lines to find the object's boundaries. Their method can be categorized as an edge-based approach because it searches for the strongest edge pixels along a set of lines normal to the contour front. These normal lines are of a pre-determined fixed length and assumed to lead to the object boundary. The current contour point of each search line is to move to a new location where the maximum gradient magnitude is located.

As one can see, the capture range of this method is limited by the length of the search lines which is set by the user. As a result, for this method to perform effectively, the initial contour must be placed no further away from the object boundary than the length of each search line. Otherwise, some parts of the contour may not move because the length of its corresponding normal lines is too short to find any boundary candidate [12]. To solve this problem, we propose the length of the search lines to be extendable until candidate boundary pixels are found. In images with high noise content, however, the maximum gradient magnitude may not well represent the true boundary of the object and the method may mistaken highly noisy pixels as the object's boundary. To solve this problem, rather than finding just one edge pixel, we use the entire intensity profile along the search line as the criterion to find the boundary candidate. This information is regional, hence less noise sensitive.

2.2 Global Region-Based Active Contour

The well-known "Active Contour Without Edges" model (ACWE), proposed by Chan and Vese [8], is a region-based geometric active contour model that divides the image into two regions; the object and the background. The contour C is embedded as the zero level set of a signed distance function $\phi(x, y)$, i.e., $C = \{(x, y) \in \Omega : \phi(x, y) = 0\}$, where Ω is the image spatial domain. In addition, the region inside the contour is defined to be positive, i.e., $\phi(x, y) > 0$, and the region outside is defined to be negative, i.e., $\phi(x, y) < 0$. They introduce the energy functional E,

$$\begin{aligned} E(\phi) = \mu \int_{\Omega} \delta_{\epsilon}(\phi) |\nabla \phi| \, dxdy \\ + \lambda_1 \int_{\Omega} |I - R_{\text{in}}|^2 H_{\epsilon}(\phi) \, dxdy \\ + \lambda_2 \int_{\Omega} |I - R_{\text{out}}|^2 (1 - H_{\epsilon}(\phi)) \, dxdy, \end{aligned} \tag{1}$$

where μ, λ_1, and λ_2 are positive-valued weighting parameters, $I(x, y)$ is the input gray-scale image, ∇ is the gradient operator, R_{in} is the average pixel intensity of the area inside the contour, R_{out} is the average pixel intensity of the area outside contour, $H_{\epsilon}(\phi)$ is a smooth regularized Heaviside function [8] representing the pixels inside contour, $1 - H_{\epsilon}(\phi)$ is the function representing the pixels outside contour, and $\delta_{\epsilon}(\phi)$ is a smooth delta function representing the pixels on (and in the neighborhood of) the contour.

The first term in Eq. (1) is the energy that regulates the length of the contour. Minimizing this term is to smoothen the contour during deformation. The last two terms are the external energy terms. When they are minimized, the contour separates the image into object and background regions. This method uses regional information of the entire image and is based on the assumption that the image intensities are statistically homogeneous in each region. As we shall see later, this method is not suitable for segmenting heterogeneous textured object. To solve this problem, we propose a new method that utilizes only the local regional information.

3. Proposed Method

In this section, we explain our novel active contour method that navigates within the image domain toward the object boundary using local regional information on extendable search lines (LRES). The extendable search lines enable the contour to move freely so that it does not get stuck at any saddle or stationary points. Meanwhile, the searching process that uses local regional information enables the contour to segment heterogeneous textured object.

3.1 Extendable Search Lines

To search for the boundary of an object, we use an active contour whose front comprises search lines with various lengths as shown in Fig. 3 (a). For readability purpose, the figure shows just a subset of search lines whose centers spread evenly along the contour. These search lines are perpendicular to the contour front. Let each line be of length k_i pixels, $i = 1, 2, \ldots, N$ where N is the number of pixels on the contour. The length of each search line is adaptive throughout the contour evolution process. The length adaptation is influenced by the image's local information. In other words, each search line is to be gradually extended

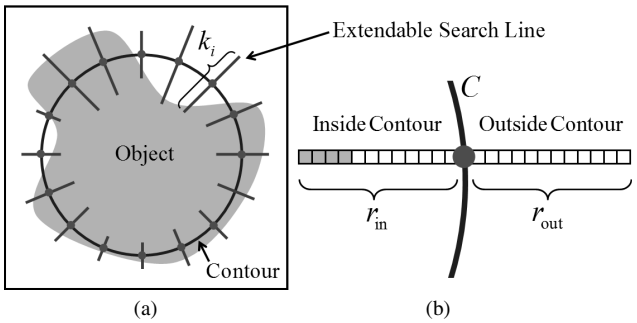

Fig. 3 Our extendable search line method.

until there is enough information to inform the contour front toward which direction to move. Therefore, in this manner, the contour can capture an object located anywhere within the image, which is opposed to the active contour with fixed-length search line that does not move if the search line does not cross any object boundary.

The local information that we are using is the image's intensity profile along the search line, as shown in Fig. 3 (b). The motion of each pixel on the contour is based on its own local regional information. The intensity profile along the search line is divided into two regions, one inside the contour and the other outside. Our method uses two local regional statistics, r_{in} and r_{out}; where r_{in} is the average pixel intensity on the part of the search line that within the contour C and r_{out} is the average pixel intensity on the part of the search line that is outside the contour C.

The search line with fixed-length cannot direct the contour if it lies entirely on a homogenous region. To solve this problem, we let the search line be of extendable length until the local regional statistics on both sides of the contour, r_{in} and r_{out}, are different; so the moving direction of the contour can be determined. The length of each line is gradually extended by η pixels from the initial length k_{start} pixels by checking whether the line lies on a homogenous region or not. In other words, if r_{in} is approximately the same as r_{out} the line's length is increased. When the line has found a heterogeneous region, supposedly the object boundary, r_{in} will be different from r_{out}. With this information, the search line can direct the contour front, which is at its center, to move toward the boundary.

3.2 Local Region-Based Force

For curve evolution, we implement our LRES active contour method via level set [17]. The advantage of this technique is that it can automatically handle any topological change during the deformation. We start by embedding a region-based force in each search line, so the local region-based energy functional of each search line, E_{line} is as in Eq. (2).

$$E_{\text{line}}(\phi) = \int_{\Omega} (I - r_{\text{in}})^2 M \cdot H_{\epsilon}(\phi) dxdy + \int_{\Omega} (I - r_{\text{out}})^2 M \cdot (1 - H_{\epsilon}(\phi))\, dxdy \qquad (2)$$

In Eq. (2), I is the input image, $H_{\epsilon}(\phi)$ is a smooth regularized Heaviside function, r_{in} and r_{out} are the average pixel intensity values on the part of each search line that are inside and outside the contour, which can be obtained using Eq. (3) and (4), respectively, and M is a line mask function for each search line as in Eq. (5).

$$r_{\text{in}} = \frac{\int_{\Omega} I \cdot M \cdot H_{\epsilon}(\phi)\, dxdy}{\int_{\Omega} M \cdot H_{\epsilon}(\phi)\, dxdy}, \qquad (3)$$

$$r_{\text{out}} = \frac{\int_{\Omega} I \cdot M \cdot (1 - H_{\epsilon}(\phi))\, dxdy}{\int_{\Omega} M \cdot (1 - H_{\epsilon}(\phi))\, dxdy}. \qquad (4)$$

$$M(x,y) = \begin{cases} 1, & (x,y) \text{ is on the search line} \\ 0, & \text{otherwise} \end{cases} \qquad (5)$$

There are two terms in our total energy as in Eq. (6),

$$E_{\text{total}}(\phi) = \mu \int_{\Omega} \delta_{\epsilon}(\phi) |\nabla\phi|\, dxdy + \nu \int_{\Omega} \delta_{\epsilon}(\phi) E_{\text{line}}(\phi)\, dxdy, \qquad (6)$$

where μ and ν are positive-valued weighting parameters, and $\delta_{\epsilon}(\phi)$ is a smooth delta function. The first term of Eq. (6) is associated with the contour length. Minimizing it is equivalent to smoothing the contour itself. The second term is our local region-based energy of all the search lines along the contour. Minimizing it implies a separation of similar textures "locally" by the contour.

Taking the derivative of Eq. (6) with respect to ϕ and equating it to $\frac{\partial\phi}{\partial t}$, we have the evolution equation of our LRES method as shown in Eq. (7), where $\kappa = \text{div}\left(\frac{\nabla\phi}{|\nabla\phi|}\right)$ is the contour's curvature. The first term is the smoothing force to control the elasticity of the contour during the deformation. The second term is our local region-based force, F_{LR}, as in Eq. (8) (see more details in the Appendix). This force acts as a driver to move the center of each search line, which is the contour, in the direction perpendicular to the contour front.

$$\frac{\partial\phi}{\partial t} = \delta_{\epsilon}(\phi)\left[\mu\kappa + F_{\text{LR}}\right] \qquad (7)$$

$$F_{\text{LR}} = \nu \int_{\Omega} \delta_{\epsilon}(\phi) M \left[-(I - r_{\text{in}})^2 + (I - r_{\text{out}})^2\right] dxdy \qquad (8)$$

3.3 Deformation Process

In this subsection, we describe the deformation process of our LRES active contour method. First of all, the initial contour is set and embedded as the zero level of the initial signed distance function, ϕ_0. Then, the search lines are formed at each pixel on the contour. Each search line is perpendicular to the contour front and its center is at the pixel on the contour. Therefore, the number of search lines, N, is equal to the number of the pixels on the contour. The length

of each search line is initially set to $k_i = k_{\text{start}}$ pixels, where $i = 1, 2, \ldots, N$. Then, two important parameters on each search line are computed, i.e., r_{in} and r_{out}. We check the condition $|r_{\text{in}} - r_{\text{out}}| < (L \times th)$ for every search line, where $th \in [0, 1]$ is a percentage of the intensity value range of the input image. For example, if the input images are 8-bit gray scale, we use $L = 255$. The value of th also refers to a small amount of threshold to indicate that r_{in} is different from r_{out}. Ideally, the value of th is to be kept closed to zero. If the condition is true, i.e., r_{in} is not much different from r_{out}, this implies that the search line is lying entirely on a homogenous region. In other words, the search line has not found any part of the object's boundary. In this case, the length of the search line is extended by setting $k_i = k_i + \eta$, where η is the step-length. After each search line has found its optimal length, where the condition $|r_{\text{in}} - r_{\text{out}}| < (L \times th)$ is not met, i.e., r_{in} is different from r_{out} by th percentage, the contour is deformed by one iteration using our evolution equation in Eq. (7). Next, the length of each search line is reinitialized to k_{start} for each new iteration. Then the whole process is iterated until the contour converges to the object boundary. Note that the number of search line in each iteration changes depending on the number of pixels on the contour in each iteration. The overall process of our active contour method has six steps as follows:

Step 1: Initialize ϕ_0 where the contour C is embedded.

Step 2: Initialize the length of each search line k_i to k_{start} pixels.

Step 3: Compute the average intensity value of the intensity profile along the region of the search line that lies inside and outside the contour, r_{in} and r_{out}, respectively.

Step 4: Check the condition $|r_{\text{in}} - r_{\text{out}}| < (L \times th)$ for every search line. If it is true, go to Step 5, otherwise go to Step 6.

Step 5: Set $k_i = k_i + \eta$ and return to Step 3 until the search line finds the object's boundary.

Step 6: Deform the contour by one iteration using our evolution equation in Eq. (7). If the contour converges, the process is done; otherwise go to Step 2.

4. Experiments

In this section, we test the performance of our active contour method proposed in Sect. 3 and compare it to both the edge-based and the region-based active contours. In all experiments, we use $\mu = 0.5$ (for the smoothing force), $\nu = 1$ (for our local region-based force), $L = 255$ (the input images are 8-bit gray scale), $th = 0.1$ (for extendable search line process), $k_{\text{start}} = 11$ pixels (5 pixels on each side of the search line and 1 pixel on the contour), and $\eta = 2$ pixels (one pixel is extended on each side of the search line) for our active contour model. The size of all tested images is 100×100 pixels.

4.1 LRES Method vs. Edge-Based Active Contours

We compare our LRES method to five previously mentioned edge-based active contours, i.e., the traditional active contour (TAC) [1], the distance vector flow (DVF) [2], the gradient vector flow (GVF) [3], the Coulomb active contour (CAC) [5], and the vector field convolution (VFC) [4] methods. These methods are implemented via level set using MATLAB. The edge map is generated by the gradient magnitude of the convolution between the input image and the Gaussian function. The thickness of the edge map depends on the variance σ^2 of the Gaussian kernel. In this experiment, we use $\sigma = 1$ for all input images. The weighting parameter for the smoothing force is set to be the same as the one used in our method, i.e., $\mu = 0.5$. The weighting parameter for the external force, ν, is also set to 1 which is similar to the one used in our method. Furthermore, the vector field of all five methods is normalized.

There are 49 images in Fig. 4, arranged into 7 rows and 7 columns. In the first row, the seven tested images, with their own initial contours, can be categorized into two types: synthetic and real scenes. The first three columns (a) to (c) are synthetic images consisting of a U shape image, a U shape image with a small opening to the concave part, and an S shape image, respectively. The last four columns (d) to (g) are real scene images. They are a flight jet image, a magnetic resonance image of a brain, a fish image, and a cardiac magnetic resonance image (CMRI), respectively. The second to the seventh rows are the final segmentation results of the TAC, DVF, GVF, CAC, VFC, and our LRES methods, respectively.

We can see in column (a) of Fig. 4 that the TAC and the DVF methods cannot segment the U shape completely because the TAC has limited capture range and the DVF does not have an ability to handle a concave shape. However, the GVF, the CAC, and the VFC methods can segment the U shape image successfully because they are capable of reaching into concave parts. Another reason why the three methods succeed in segmenting the U shape is that there are no saddle or stationary points in this case. Our method also provides a perfect segmentation result. As mentioned in Sect. 3.1, using extendable search lines enables our active contour to have large capture range and an ability to move into the concave part of the object.

In column (b), we can see that all five edge-based active contours stop at the small opening of the concave part of the U shape. The contours did not move into the "bay" region due to the existence of the saddle and stationary points. As shown in Fig. 1 (c), the stationary point at the "bay" region results in a saddle point at the "bottleneck" region. This saddle point behaves as a "wall" that obstructs the active contour to pass inside. Our active contour method as shown in the last row, however, can reach into the deep concave part because we use search lines rather than a vector field. Similarly, the S shape image in column (c) cannot be successfully segmented using all of the five edge-based methods. These methods fail because the saddle and stationary points appear in the both "bay" regions of the S shape. However, our LRES method in the last row can segment the S shape accurately.

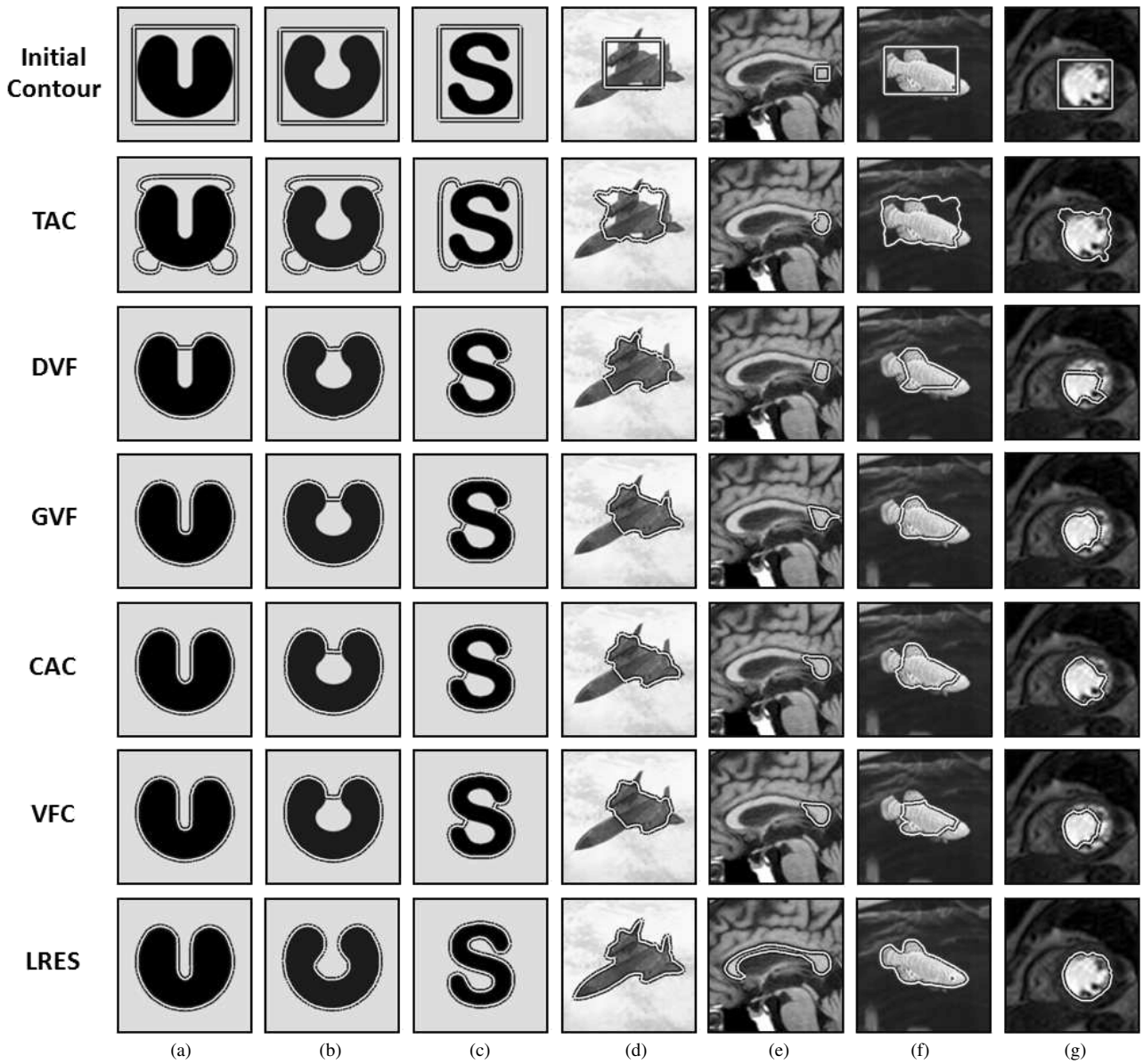

Fig. 4 Comparison with the edge-based active contours. First row: initial contour. Second to seventh rows: segmentation results by using the TAC, DVF, GVF, CAC, VFC, and our LRES methods, respectively.

Furthermore, the saddle and stationary points may inevitably appear in real scene images. In column (d), for example, when we place the initial contour around the rear end of the flight jet, all five edge-based active contours cannot reach the cockpit due to a stationary point at the head part of the flight jet. However, this is not a problem for our method. Our active contour can conveniently move to the head part of the flight jet and provides a desirable segmentation result as shown in the last row. Another example is shown in column (e). We place the initial contour on the right of the corpus callosum. All five edge-based methods suffer a saddle point located on the right during the deformation. Thus, the contour cannot segment the overall of the corpus callosum. In contrast, our LRES method can segment the desired corpus callosum completely as shown in the last row.

In column (f), a fish image is tested. We found that all five edge-based forces move the contour front to the pixels on the heterogeneous texture of the fish rather than the true boundary of the fish itself because the fish's heterogeneous texture has stronger gradient magnitude than the boundary pixels. We notice further that all five edge-based contours are stuck at the fish eye because it is of the highest gradient in the image as shown in Fig. 5 (a), resulting in a vector field, as shown in Fig. 5 (b) and (c), that is pointing to the fish eye rather than the fish's boundary. Our LRES active contour, on the other hand, can move beyond the fish eye because our local region-base force considers the eye pixel as merely a noisy pixel compared to other intensity values on the search

line. Therefore, the eye pixel does not have much influence on our local region-based search line.

The last tested image is the cardiac magnetic resonance image as shown in column (g) of Fig. 4. This image has high content of noise causing spurious edges that confuse all five edge-based active contours during the deformation. In addition, the papillary muscles inside the left ventricular region and other tissues outside the heart further obstruct the contour to find the true boundary of the left ventricle. Our LRES contour, on the other hand, can trace the actual left ventricular boundary correctly. In summary, testing our local region-based active contour scheme on the fish and the cardiac magnetic resonance images verifies that our LRES method is less sensitive to noise than the edge-based active contours. In conclusion, our active contour method performs better than the edge-based ones in the sense that it has a large capture range, an ability to handle concave shapes, no existence of the saddle and stationary point problems, and robustness to noise.

4.2 LRES Method vs. Region-Based Active Contour

4.2.1 Comparison with Global Region-Based Method

In this subsection, we are comparing our local region-based active contour to the global region-based one proposed by Chan and Vese (ACWE method) [8]. In Eq. (1), there are three weighting parameters for ACWE method. We set $\mu = 0.5$ for the smoothing force which is similar to other methods and $\lambda_1 = \lambda_2 = 1$ for the external force.

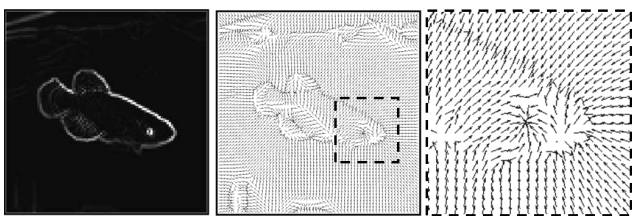

(a) (b) (c)

Fig. 5 (a) the edge map of the fish image (b) the VFC vector filed and (c) the VFC vector filed at the eye part of the fish image.

Figure 6 is divided into 3 rows and 7 columns. Two synthetic images and five real scene images are used to compare our proposed LRES active contour to the ACWE. In column (a), a triangular-like object with homogeneous texture is placed in a uniform background. In column (b), the same triangular shape object as (a) but with heterogeneous texture is placed in a background with non-uniform intensity. Column (c) to (g) are real scence images consisting of a balloon, a flower, a teddy bear, an image with two cats and a brain tumor magnetic resonance image [13], respectively.

For the homogeneous texture object in column (a), we found that both ACWE and LRES methods can successfully segment the triangular-like object. This object is easy to segment by both methods because the intensity of the object and the background are clearly different. For the heterogeneous texture object in column (b), however, our local region-based active contour can still segment it correctly while the ACWE fails. In this image, the intensity of both the object and the background areas is non-uniform. Since the global region-based active contour attempts to separate the dark region from the lighter one, the result is that the dark regions of both object and background are grouped together as one and the light regions of both areas are considered as the other object. However, the LRES method, a local region-based active contour, can distinguish the difference in intensity locally. Therefore, it can find the true object boundary successfully even though the object and the background are of non-uniform intensities. The balloon image in column (c) also has heterogeneous texture. The global region-based method cannot segment the complete balloon shape because some parts of the balloon have intensity that

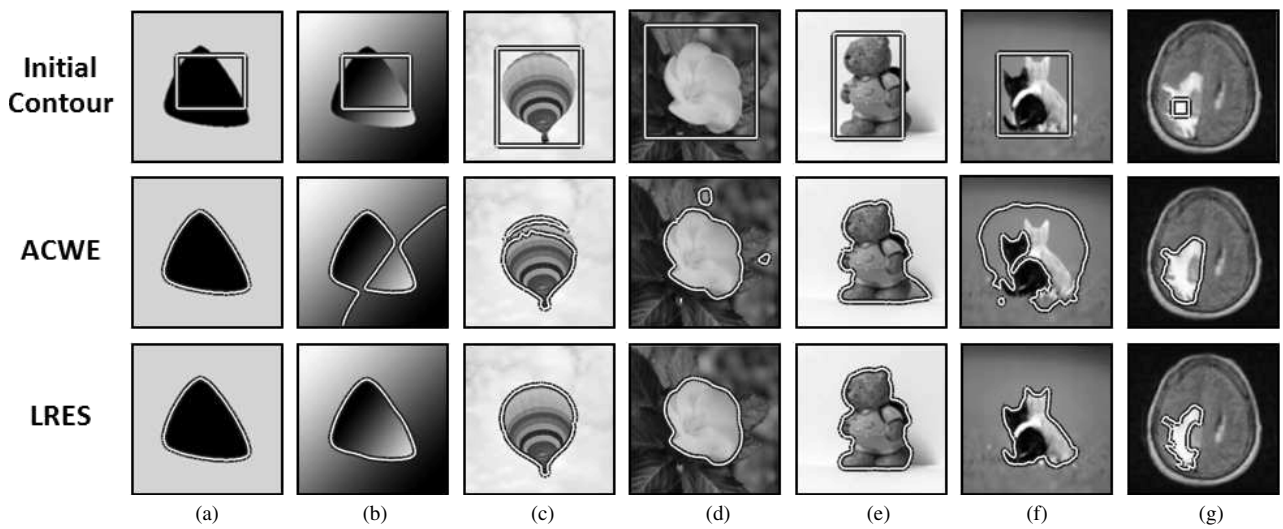

Fig. 6 Comparison with the global region-based active contour. First row: initial contour. Second and third rows: segmentation results by using the ACWE and our LRES methods, respectively.

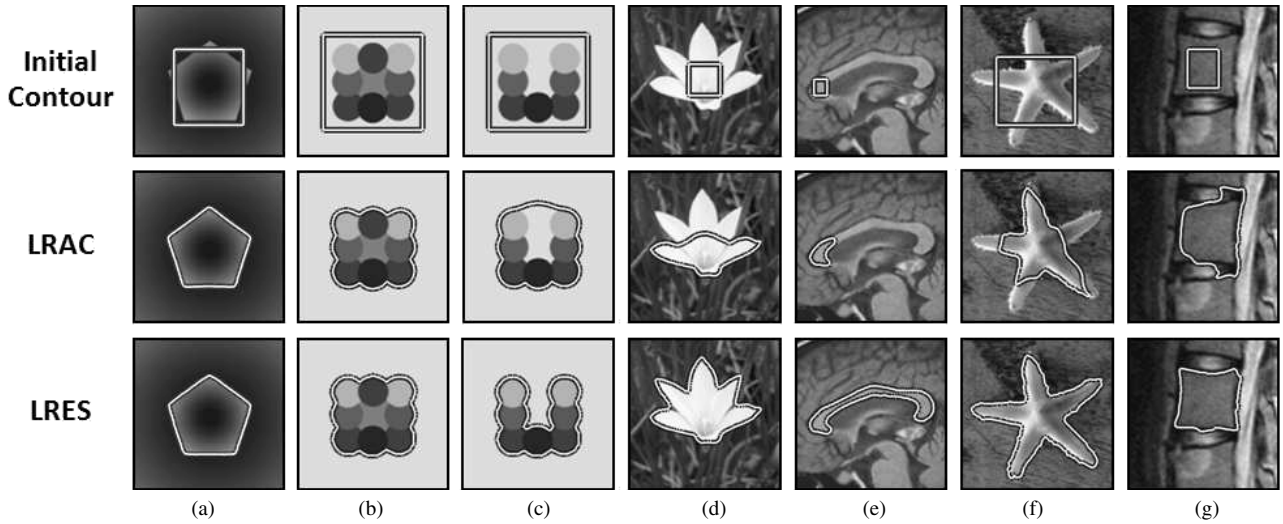

Fig. 7 Comparison with the local region-based active contour. First row: initial contour. Second and third rows: segmentation results by using the LRAC and our LRES methods, respectively.

is similar to the sky which is in the background. However, our method can effectively provide the whole part of balloon shape due to our local region-based force.

For the flower image in column (d), we can see that even though the global region-based method can trace the boundary of the flower correctly, it also includes some small non-flower-regions. This is because those regions have about the same intensity as the flower region. On the other hand, our method traces only the flower boundary because it searches only locally in the vicinity of flower. For the teddy bear image in column (e), the global region-based active contour not only traces the boundary of the bear itself but also includes its shadow, appeared behind the leg. The LRES active contour, on the other hand, correctly traces just the desired bear and not its shadow. For the two cats, one black and one white, in column (f), the global region-based active contour separates the black cat from the white one because they have entirely different textural intensity. Nonetheless, our LRES active contour segments both cats as one object even though their textures are different. Again this is due to the local regional information of the LRES method.

In column (g), we want to segment the brain tumor in a magnetic resonance image, so the initial contour is placed within the tumor region. We can see that the tumor is of heterogeneous texture object. Therefore, the global region-based method cannot successfully segment this tumor. A more satisfactory result, as shown in the last row, is provided by our local region-based LRES method. In conclusion, all of the experiments in this subsection have shown that our new LRES active contour with local regional statistics performs well on heterogeneous object segmentation compared to the global region-based counterpart.

4.2.2 Comparison with Local Region-Based Method

In this subsection, we are comparing our LRES active contour to another local region-based one, proposed by Lankton and Tannenbaum (LRAC method) [16]. The MATLAB code of this method is provided by the authors [16]. Similar to other methods, we set the weighting parameter for the smoothing force to 0.5. Furthermore, the important parameter of this method is the radius of the circles that covers the local region. The radius parameters of all circles around the contour have the same size and unchanged during the deformation. The default size is set to be approximately 1/10 of the input image size. In the experiment, all input images are 100×100, so the radius parameter is defined to be 10 pixels.

Figure 7 is divided into 3 rows and 7 columns. Three synthetic images and four real scenes are used in this experiment. In column (a), a pentagon object with heterogeneous texture. In column (b), a group of nine circles with different shades arranged as a square-like shape. In column (c), a group of seven circles arranged as a U shape. Column (d) to (g) are real scenes images consisting of a flower, a corpus callosum, a starfish and a vertebra MRI image, respectively.

For the heterogeneous texture object in column (a), both LRAC and our LRES methods can segment the pentagon object perfectly. This object can be segmented easily because the initial contour is placed nearby the object's boundary and both methods utilize the local regional information to drive the active contour. Another type of the heterogeneous texture object is tested in column (b). We found that both LRAC and our LRES methods can successfully segment this object. Next, the U shape object in column (c) is tested. The initial contour is placed outside the object as shown in the first row. We can see that the LRAC method can not segment the U shape completely because it has poor capture range when the radius parameter is too

small. To increase the capture range for the LRAC method, we change the radius parameter to 20, 30, and 40 pixels whose results are shown in Fig. 8 (a), (b), and (c), respectively. We can see in Fig. 8 (a), when the radius parameter is set to 20 pixels, the contour moves somewhat toward the opening of the U shape but still cannot reach the inner part of the U shape. This is because the size of the radius also is not large enough. We then increase the radius parameter to 30 pixels. The contour can move toward the innermost part of the U shape; however, the top two light shaded circles are neglected. As a result, it cannot completely segment the desired U shape. In this case, the larger radius enables the LRAC method to behave a little more like a global region-based active contour, so the top two light shaded circles are classified as a part of the background. We can clearly see this effect when we set the radius parameter to 40 pixels, where the next two slightly darker shaded circles are grouped together as a part of the background too. In contrast, our LRES method employs the extendable search lines and each individual line has its own length. Therefore, our LRES contour can move toward the innermost part of the U shape without considering the differently shaded circles as different objects or a part of the background. Therefore, the U shape can be segmented perfectly by our LRES method as shown in the last row of Fig. 7 (c).

For the real scene image of a flower in column (d), the initial contour is placed inside the flower. The segmentation result of the LRAC method covers only three of the six flower's petals. Our LRES method, on the other hand, can correctly trace all six petals, which are the actual flower's boundary. For the corpus callosum image in column (e), the initial contour is placed to the left of the corpus callosum. The LRAC contour in the second row cannot segment the overall part of the corpus callosum. However, the contour with extendable capture range of our LRES method can move toward the right end of the corpus callosum perfectly. Another example in column (f), we place the initial contour on the middle part of the starfish. We found that the LRAC method fails to segment the starfish correctly because of its limited capture range. As a result, the LRAC contour cannot reach into some protruding ends of the starfish. In contrast, our LRES contour can segment the whole part of the starfish completely.

In column (g), we want to segment only one vertebra in the image, so the initial contour is placed inside the desired vertebra region. We can see that the LRAC contour in the second row has some spill-over regions on the top and the bottom parts on the right while our LRES contour can trace the vertebra more accurately. This is because the LRAC method uses the intensity inside a circle, not just on the (normal) search line like the LRES does. This implies that all neighborhood pixels around the point on the contour have influenced the contour evenly. In other words, the contour tends to spread all around, not just in the normal direction. As a result, the segmentation region is easy to have a spill-over. In contrast, our LRES method, which uses only the intensity profile along search lines that are normal to the contour. Therefore, our LRES contour can segment the vertebra correctly without spreading over to undesirable region. In other words, our LRES method utilizes the regional information more locally than the LRAC method. In summary, our LRES active contour performs better than the LRAC method in the sense that it has a large capture range, an ability to segment concave shapes without mutating to be a global type.

4.3 Test of Convergent Rate

In this subsection, we are to study the convergent rate of our LRES method compared to the VFC (an edge-based method), the ACWE (a global region-based method), and the LRAC (a local region-based method). All methods are implemented via level set using MATLAB on a 2.40 GHz Core 2 Duo processor with a 4 GB RAM. The image used is the triangular-like shape object with the initial contour shown in column (a) of Fig. 6. The maximum number of iterations for each method is set to 100. In each iteration, the evolving contour C_t is compared to the desired final contour C_f, i.e., the triangular-like shape, using the area similarity measurement [20], $S_{area} \in [0, 1]$ as in Eq. (9),

$$S_{area} = \frac{2n\left(C_t \wedge C_f\right)}{n\left(C_t\right) + n\left(C_f\right)}, \tag{9}$$

where $n\left(C_t \wedge C_f\right)$ is the number of pixels inside both C_t and C_f, $n\left(C_t\right)$ is the number of pixels inside C_t and $n\left(C_f\right)$ is the number of pixels inside C_f. If S_{area} is equal to 1, it implies that both C_t and C_f have the same shape.

The area similarity values of each method through out 100 iterations are shown in Fig. 9. We can see that, to converge to the desired shape, the VFC, the ACWE, and the

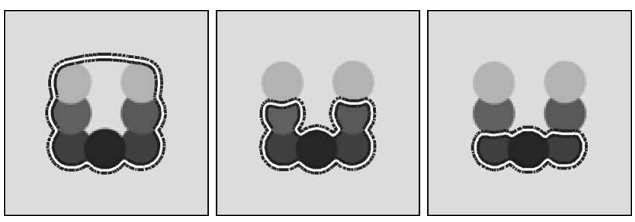

(a) (b) (c)

Fig. 8 The segmentation results by using the LRAC method [16] when the radius parameter is set to (a) 20, (b) 30, and (c) 40 pixels, respectively.

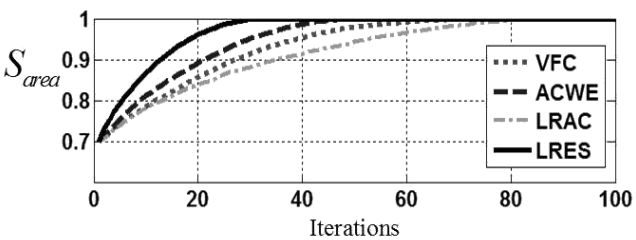

Fig. 9 The convergent rate of the VFC, the ACWE, the LRAC, and our LRES methods.

LRAC methods require approximately 70, 47, and 80 iterations, respectively. Meanwhile, our method requires only 30 iterations to converge to the desired object. However, we found that the VFC, the ACWE, the LRAC, and our LRES methods require approximately 0.061, 0.062, 0.157, and 0.302 second per one iteration, respectively. This results in a total computational time of 4.27, 2.914, 12.56, 9.06 second for VFC, ACWE, LRAC, and LRES, respectively. As it turns out, our LRES method requires slightly more computational time than that of the VFC and ACWE methods. This is not surprising because our LRES method requires additional processing of extending search line for each iteration. In such process, each search line needs to find its own optimum length by increasing its length gradually until the object's boundary is found. A more relevant comparison is between our LRES method and the LRAC method, both of which need additional computation on local regional information. When benchmarked with the LRAC method, our LRES method acquires less overall computational time, yet can deliver better segmentation performances. Moreover, we can further reduce the computation time of our LRES method by implementing it using C++. We found that our LRES method requires only 0.015 second per one iteration in C++.

5. Conclusion

A novel active contour called the LRES method that uses local regional statistics on extendable search lines has been proposed in this paper. We design each search line to be of adaptive length so that it can navigate the contour front toward the object boundary with extendable capture range. The intensity profile of the pixels along a set of search lines, which are normal to the contour front, are used to compute our local regional force, enabling the contour to segment object with heterogeneous texture. From our experiments, the advantages of our method over the edge-based active contours are a large capture range, an ability to reach into deep concave shape, no existence of the saddle and stationary point problems, and robustness to noise. When compared to an active contour with global regional force, our method performs better in segmenting heterogeneous textured objects. Furthermore, when compared to another local region-based active contour such as LRAC, our LRES method does not need to priori set any capture range parameter because it is automatically adaptive and it also requires less overall processing time.

Acknowledgments

This work is partially supported by Thailand Graduate Institute of Science and Technology (TGIST) TG-44-09-50-083D, the research assistant grant from the Faculty of Engineering, and the 90 year Chulalongkorn Ratchdaphiseksomphoj grant from Chulalongkorn University. Moreover, the authors would like to thank Dr. Pairash Saiviroonporn, Dr. Rungroj Krittayaphong, and the Cardiac Center at Siriraj Hospital, Thailand, for providing the Cardiac MR image.

References

[1] M. Kass, A. Witkin, and D. Terzopoulos, "Snakes: Active contour models," Int. J. Comput. Vis., vol.1, no.4, pp.321–331, 1988.
[2] L.D. Cohen and I. Cohen, "Finite-element methods for active contour models and balloons for 2-D and 3-D images," IEEE Trans. Pattern Anal. Mach. Intell., vol.15, no.11, pp.1131–1147, Nov. 1993.
[3] C. Xu and J.L. Prince, "Snakes, shapes, and gradient vector flow," IEEE Trans. Image Process., vol.7, no.3, pp.359–369, March 1998.
[4] B. Li and S.T. Acton, "Active contour external force using vector field convolution for image segmentation," IEEE Trans. Image Process., vol.16, no.8, pp.2096–2106, Aug. 2007.
[5] B. Wang and L.M. Zhang, "A new snake model based on the Coulomb law," Proc. IEEE 2003 International Conference on Neural Networks and Signal Processing, Nanjing, China, pp.1113–1116, Dec. 2003.
[6] T. Wang, I. Cheng, and A. Basu, "Fluid vector flow and applications in brain tumor segmentation," IEEE Trans. Biomed. Eng., vol.56, no.3, pp.781–789, March 2009.
[7] T.F. Cootes, C.J. Taylor, D.H. Cooper, and J. Graham, "Active shape models — Their training and application," Computer Vision and Image Understanding, vol.61, no.1, pp.38–59, Jan. 1995.
[8] T.F. Chan and L.A. Vese, "Active contours without edges," IEEE Trans. Image Process., vol.10, no.2, pp.266–277, Feb. 2001.
[9] J.A. Yezzi, A. Tsai, and A. Willsky, "A fully global approach to image segmentation via coupled curve evolution equations," J. Vis. Commun. Image Represent., vol.13, no.1, pp.195–216, March 2002.
[10] O. Michailovich, Y. Rathi, and A. Tannenbaum, "Image segmentation using active contours driven by the Bhattacharyya gradient flow," IEEE Trans. Image Process., vol.16, no.11, pp.2787–2801, Nov. 2007.
[11] S. Phumeechanya, C. Pluempitiwiriyawej, and S. Sotthivirat, "3D left ventricular segmentation using double active contours and double active surfaces," The 30th Annual International Conference of IEEE Engineering in Medicine and Biology Society (EMBC 2008), pp.214–217, Vancouver, Canada, Aug. 2008.
[12] S. Phumeechanya, C. Pluempitiwiriyawej, and S. Thongvigitmanee, "Active contour using local region-based force with adaptive-length search line," The Ninth IASTED International Conference on Visualization, Imaging and Image Processing (VIIP 2009), pp.91–96, Cambridge, United Kingdom, July 2009.
[13] Y. Yang, S. Huang, P. Lin, and N. Rao, "Medical Image Segmentation based on level set combining with region information," The Fourth International Conference on Natural Computation, Jinan, China, pp.70–74, Oct. 2008.
[14] J. Mille and L.D. Cohen, "A local normal-based region term for active contours," Energy Minimization Methods in Computer Vision and Pattern Recognition, Lect. Notes Comput. Sci., vol.5681, pp.168–181, Springer Berlin Heidelberg, 2009.
[15] R. Ronfard, "Region-based strategies for active contour models," Int. J. Comput. Vis., vol.13, pp.229–251, 1994.
[16] S. Lankton and A. Tannenbaum, "Localizing region-based active contours," IEEE Trans. Image Process., vol.17, no.11, pp.2029–2039, Nov. 2008.
[17] R. Malladi, J. Sethian, and B.C. Vemuri, "Shape modeling with front propagation: A level set approach," IEEE Trans. Pattern Anal. Mach. Intell., vol.17, no.2, pp.158–175, Feb. 1995.
[18] D. Mumford and J. Shah, "Optimal approximation by piecewise smooth functions and associated variational problems," Communications on Pure and Applied Mathematics, vol.42, pp.577–685, 1989.
[19] A. Bhattacharyya, "On a measure of divergence between two statistical populations defined by their probability distributions," Bull. Calcutta Math. Soc., vol.35, pp.99–109, 1943.
[20] C. Pluempitiwiriyawej, J.M.F. Moura, Y.-J.L. Wu, and C. Ho,

"STACS: New active contour scheme for cardiac MR image segmentation," IEEE Trans. Med. Imaging, vol.24, no.5, pp.593–603, May 2005.

Appendix: Obtaining of Our Local Region-Based Force

In Sect. 3.2, we showed that the evolution equation of our LRES active contour method as in Eq. (7) consists of two terms. The first term is the smoothing force while the second term is our local region-based force, F_{LR} as in Eq. (8). To obtain our local region-based force, we minimize the second term of our total energy function in Eq. (6). We restate only the second term here:

$$E(\phi) = \nu \int_{\Omega} \delta_{\epsilon}(\phi)\, E_{\mathrm{line}}(\phi)\, dxdy, \qquad (\mathrm{A}\cdot 1)$$

where E_{line} is our local region-based energy function as in Eq. (2).

In order to minimize the energy function, we take the derivative of Eq. (A· 1) with respect to ϕ and equate it to $\frac{\partial \phi}{\partial t}$

$$\begin{aligned}\frac{\partial \phi}{\partial t} &= -\frac{\partial F}{\partial \phi} = -\frac{\partial}{\partial \phi}\left[\nu\, \delta_{\epsilon}(\phi)\, E_{\mathrm{line}}(\phi)\right] \\ &= -\nu\left[\delta_{\epsilon}(\phi)\frac{\partial}{\partial \phi}E_{\mathrm{line}}(\phi) + E_{\mathrm{line}}(\phi)\,\delta'_{\epsilon}(\phi)\right], \qquad (\mathrm{A}\cdot 2)\end{aligned}$$

where $\delta'_{\epsilon}(\phi)$ is the first derivative of $\delta_{\epsilon}(\phi)$.

We notice that, on the contour which is the zero level set, $\delta'_{\epsilon}(\phi)$ evaluates to zero. Thus, by omitting the second term of Eq. (A· 2), we only have

$$\frac{\partial \phi}{\partial t} = -\nu\, \delta_{\epsilon}(\phi)\frac{\partial}{\partial \phi}E_{\mathrm{line}}(\phi), \qquad (\mathrm{A}\cdot 3)$$

where

$$\begin{aligned}\frac{\partial}{\partial \phi}E_{\mathrm{line}}(\phi) &= \int_{\Omega}\frac{\partial}{\partial \phi}\left[(I-r_{\mathrm{in}})^2\cdot M\cdot H_{\epsilon}(\phi)\right]dxdy \\ &\quad + \int_{\Omega}\frac{\partial}{\partial \phi}\left[(I-r_{\mathrm{out}})^2\cdot M\cdot(1-H_{\epsilon}(\phi))\right]dxdy \\ &= \int_{\Omega}\delta_{\epsilon}(\phi)\, M\left[(I-r_{\mathrm{in}})^2-(I-r_{\mathrm{out}})^2\right]dxdy. \qquad (\mathrm{A}\cdot 4)\end{aligned}$$

Substituting $\frac{\partial}{\partial \phi}E_{\mathrm{line}}(\phi)$ into Eq. (A· 3), we get our local region-based force, F_{LR} as follows:

$$\begin{aligned}\frac{\partial \phi}{\partial t} &= -\nu\delta_{\epsilon}(\phi)\int_{\Omega}\delta_{\epsilon}(\phi)\, M\left[(I-r_{\mathrm{in}})^2-(I-r_{\mathrm{out}})^2\right]dxdy \\ &= \delta_{\epsilon}(\phi)\left(\nu\int_{\Omega}\delta_{\epsilon}(\phi)\, M\left[-(I-r_{\mathrm{in}})^2+(I-r_{\mathrm{out}})^2\right]dxdy\right) \\ &= \delta_{\epsilon}(\phi)\, F_{\mathrm{LR}} \qquad (\mathrm{A}\cdot 5)\end{aligned}$$

$$F_{\mathrm{LR}} = \nu\int_{\Omega}\delta_{\epsilon}(\phi)\, M\left[-(I-r_{\mathrm{in}})^2+(I-r_{\mathrm{out}})^2\right]dxdy. \qquad (\mathrm{A}\cdot 6)$$

Sopon Phumeechanya received the B.Eng. degree in Electronics and Telecommunication Engineering from King Mongkut's University of Technology Thonburi, Bangkok, Thailand in 2005, and the M.Eng. degree in Electrical Engineering from Chulalongkorn University, Bangkok, Thailand in 2007. He is currently working toward his Ph.D. degree in Electrical Engineering at the Department of Electrical Engineering, Chulalongkorn University. His research interests include image segmentation, computer vision, and 3D image reconstruction.

Charnchai Pluempitiwiriyawej received the B.S. degree in Electrical Engineering from University of Maryland at College Park in 1995, and the M.S. and Ph.D. degrees from the Department of Electrical and Computer Engineering, Carnegie Mellon University, Pittsburgh, Pennsylvania in 1997 and 2004, respectively. He is currently an assistant professor at the Department of Electrical Engineering, Chulalongkorn University, Bangkok, Thailand. His research interests include medical image segmentation using active contour, level set method, 3D image reconstruction.

Saowapak Thongvigitmanee received the B.S. degree in Electrical Engineering from Cornell University, USA in 1997, and the M.S. and Ph.D. degrees in Electrical Engineering: Systems from the University of Michigan, Ann Arbor, USA in 1998 and 2003, respectively. Since 2003, she has been working at the National Electronics and Computer Technology Center (NECTEC). Her research interests include image processing, signal processing, and medical imaging. In 2008, she won Thailand Young Technologist Award from the Foundation for the Promotion of Science and Technology under the Patronage of H.M. the King.